Hypertension Research (2013) 36, 770–775

www.nature.com/hr

ORIGINAL ARTICLE

Non-invasive assessment of cardiac function in a mouse model of renovascular hypertension

Federico Franchi[1], Bruce E Knudsen[2], Elise Oehler[1], Stephen C Textor[2], Lilach O Lerman[2], Joseph P Grande[3] and Martin Rodriguez-Porcel[1]

Hypertension continues to be a significant cause of morbidity and mortality, underscoring the need to better understand its early effects on the myocardium. The aim of this study is to determine the feasibility of *in vivo* longitudinal assessment of cardiac function, particularly diastolic function, in a mouse model of renovascular hypertension. Renovascular hypertension (RVH) was induced in 129S1/SvImJ male mice ($n=9$). To assess left ventricular (LV) systolic and diastolic function, M-mode echocardiography, pulsed-wave Doppler echocardiography and tissue Doppler imaging were performed at baseline, 2 and 4 weeks after the induction of renal artery stenosis. Myocardial tissue was collected to assess cellular morphology, fibrosis, extracellular matrix remodeling and inflammation *ex vivo*. RVH led to a significant increase in systolic blood pressure after 2 and 4 weeks (baseline: 99.26 ± 1.09 mm Hg; 2 weeks: 140.90 ± 7.64 mm Hg; 4 weeks: 147.52 ± 5.91 mm Hg, $P<0.05$), resulting in a significant decrease in LV end-diastolic volume, associated with a significant elevation in ejection fraction and preserved cardiac output. Furthermore, the animals developed an abnormal diastolic function profile, with a shortening in the E velocity deceleration time as well as increases in the E/e′ and the E/A ratio. The *ex vivo* analysis revealed a significant increase in myocyte size and deposition of extracellular matrix. Non-invasive high-resolution ultrasonography allowed assessment of the diastolic function profile in a small animal model of renovascular hypertension.
Hypertension Research (2013) **36,** 770–775; doi:10.1038/hr.2013.43; published online 16 May 2013

Keywords: cardiac function; echocardiography; fibrosis; hypertension; inflammation

INTRODUCTION

Systemic hypertension is a major cardiovascular risk factor and affects a large proportion of the adult population, including 70% of patients over 65 years of age.[1] Renovascular hypertension (RVH) is the most common secondary cause of systemic hypertension,[1,2] and thus there is significant interest in studying its pathophysiology and impact on target organs like the heart. Over the last 30 years, there have been significant advances in understanding the pathophysiological effects of RVH, leading to better insights into therapeutic strategies for RVH, especially targeting cardiac function and remodeling.[3–7] However, hypertension-induced cardiac disease continues to cause significant morbidity and mortality, underscoring the need to further understand the early myocardial implications of this common disease.

The Goldblatt two-kidney, one-clip (2K1C) hypertension model[8] is long established and widely employed in the study of RVH in different animal models,[9–11] providing a highly reproducible and clinically relevant model of systemic hypertension, which greatly contributed to our knowledge of cardiovascular disease. Our group has recently described a detailed temporal analysis of candidate genes and proteins that are involved in critical renal signaling pathways, such as cell proliferation, cell death, epithelial–mesenchymal transformation and fibrosis, that are activated in a murine model of 2K1C hypertension.[12] Furthermore, RVH has been described to be associated with the activation of pro-fibrotic pathways,[13] which in turn is accompanied by an increase in cardiac mass (LV hypertrophy)[14] leading to myocardial remodeling. A clear understanding of the effect that RVH has on the myocardial microenvironment, which will impact LV systolic and diastolic function, will be critical to better delineate disease progression and to monitor therapy.

To better investigate the impact of RVH in the heart and assess the effect of novel therapeutics, it is important to develop imaging strategies to non-invasively monitor the progression of the disease. In small animal studies, echocardiography has been long used to assess cardiac systolic function.[15,16] Novel developments in high-resolution ultrasonography now permit extension of these investigations into a more complete assessment of cardiac function, which can provide insights into earlier stages of RVH in small animal models, permitting a better and more comprehensive understanding of the impact of RVH in the heart.

Thus, using a murine model of 2K1C,[12,17] the present study was undertaken to evaluate the feasibility of non-invasive *in vivo* longitudinal assessment of cardiac systolic and diastolic function in murine RVH, and to correlate them with *ex vivo* assessment of different biological factors involved in the myocardium of RVH animals.

[1]Department of Internal Medicine, Divisions of Cardiovascular Diseases, Mayo Clinic, Rochester, MN, USA; [2]Division of Nephrology and Hypertension, Mayo Clinic, Rochester, MN, USA and [3]Department of Laboratory Medicine and Pathology, Mayo Clinic, Rochester, MN, USA
Correspondence: Dr M Rodriguez-Porcel, Department of Internal Medicine, Divisions of Cardiovascular Diseases, Mayo Clinic, 200 First Street SW, Rochester, MN 55905, USA.
E-mail: Rodriguez.m@mayo.edu
Received 9 October 2012; revised 22 January 2013; accepted 14 February 2013; published online 16 May 2013

MATERIALS AND METHODS

Animals

Studies were performed on male 129S1/SvImJ mice (Jackson Laboratory, Bar Harbour, ME, USA) of 6–7 weeks of age, weighing 20–25 g.[12] All animal procedures were performed in accordance with the National Institutes of Health *Guide for the Care and Use of Laboratory Animals*, and the Mayo Clinic College of Medicine Institutional Animal Care and Use Committee approved the study protocol.

Study outline

Mice underwent a surgical procedure for the induction of RVH by renal artery stenosis.[12] LV systolic and diastolic functions as well as blood pressure (BP) measurements were assessed 3 days before and then 2 and 4 weeks after induction of renal artery stenosis. At 4-week post surgery, mice were euthanized and tissue collected for *ex vivo* studies.

Surgical procedure

For the induction of RVH in mice ($n = 9$), we used a modified approach to the standard Goldblatt 1-clip-2-kidney model, traditionally done by placement of a silver clip to partially occlude the renal artery.[8,16,18] For these studies, we placed a small polyetrafluoroethylene cuff (outer diameter = 0.36 mm × internal diameter = 0.2 mm × L 0.5 mm) around the right renal artery to induce renal artery stenosis and subsequent systemic hypertension.[12] Briefly, mice were anesthetized with isoflurane (1.75%), the lateral skin shaved and wiped clean with topical antiseptic and alcohol, and the right kidney exposed through a small flank incision 1 cm in length. The renal artery was then exposed and a short segment dissected free of the renal vein. A polyetrafluoroethylene cuff (outer diameter = 0.36 mm × internal diameter = 0.2 mm × L 0.5 mm) was placed around the renal artery (0.25 mm in diameter, as assessed by ultrasound) and secured with two 10-0 nylon sutures. The abdominal cavity was closed in two layers (muscle and skin) with a 6-0 Vicryl suture.

Mice recovered from anesthesia on 37 °C pad until ambulatory and then returned to routine housing. After a 2-week acclimatization period, systolic, diastolic and mean arterial blood pressure were assessed at three time points (3 days before, 2 weeks and 4 weeks after surgery) by the tail-cuff method using the XBP1000 non-invasive blood pressure system (CODA system, Kent Scientific, Torrington, CT, USA).[12,19] At 4 weeks, the mice were euthanized, the heart was harvested and fixed for histopathological analysis and immunohistochemical staining.

Echocardiography

Two-dimensional, Doppler and M-mode echocardiography acquisitions were performed at baseline (3 days before surgery), 2 and 4 weeks after the induction of RVH with a high-resolution ultrasound system (Vevo 770, VisualSonics, Toronto, ON, Canada),[20] equipped with a 30-MHz mechanical transducer. Animals were anesthetized with 1.5% of isoflurane during the whole procedure (25–30 min) and placed on a warming platform (set to 38 °C) in a supine position. The animal's heart rate, ECG signal and respiration rate were recorded, and the body temperature monitored. The chest was shaved and further cleaned with a depilatory cream to minimize signal interference. Aquasonic 100 gel (Parker Laboratories, Fairfield, NJ, USA) was applied to the thorax surface to optimize visibility of the cardiac chambers.[20] Parasternal long-axis, parasternal short-axis and apical four-chamber two-dimensional views were acquired.

For the assessment of LV systolic function, the M-mode of the parasternal long- and short-axis views at the papillary muscle level was used (Figures 1a and b). In these views, the parameters calculated were: LV muscle mass ($[1.053 \times ((LVIDd + LVPWd + LVAWd)^3 - LVIDd^3)] \times 0.8$, where LVIDd represents the LV internal diameter at end-diastole, LVPW and LVAW represent LV posterior or anterior wall thickness and 1.053 is the specific gravity of muscle, LV end-systolic and end-diastolic volumes ($\mathrm{LVESV} = \left(\frac{7.0}{(2.4 + \mathrm{LVIDs})}\right) \times \mathrm{LVIDs}^3$, $\mathrm{LVEDV} = \left(\frac{7.0}{(2.4 + \mathrm{LVIDd})}\right) \times \mathrm{LVIDd}^3$), as well as LV ejection fraction (LVEF), expressed as the fraction of blood volume ejected after each heart beat ($\frac{(\mathrm{EDV} - \mathrm{ESV})}{\mathrm{EDV}} \times 100$), and cardiac output (CO) $\frac{[(\mathrm{EDV} - \mathrm{ESV}) \times \mathrm{HR}]}{1000}$.[21–23]

For the assessment of diastology, an apical four-chamber view was acquired by positioning the transducer as parallel to the mitral inflow as possible (Figure 1c). Tissue motion velocity was assessed by spectral pulsed-wave Tissue Doppler imaging, obtained from the mitral septal annulus.[24] LV diastolic function was assessed by the measurement of the LV transmitral early peak flow velocity (E) to LV transmitral late peak flow velocity (A) wave ratio, the deceleration time, the E to e' (mitral annulus early diastole tissue motion) wave ratio.[25,26] Flow velocity recordings were performed by pulsed-wave spectral Doppler imaging setting the sample volume close to the tip of the mitral leaflets. Images and Doppler measurements were obtained from at least three consecutive cycles, such that the E and A waves were separated optimally and the E wave recorded was a maximum. Deceleration time measurements were corrected for heart rate differences by dividing respective values by the square root of the R-R interval.[27]

Immunohistochemical staining

Heart tissues were fixed in 10% neutral buffered formalin, dehydrated and embedded in paraffin and histologic sections (4 μm thick) were prepared. Representative sections were stained with hematoxylin and eosin for whole LV size and structure and myocyte size; and Masson's Trichrome stain for fibrosis. Additional unstained slides were prepared for immunohistochemical staining including Collagen III and a macrophage marker (F4/80). Antigen retrieval was performed by heat treatment in citrate buffer for 20 min, using a commercial vegetable steamer for the F4/80 stain. Enzyme treatment (trypsin, 15 min at 37 °C) was used for the Collagen III stain. Primary and secondary antibodies used were: goat anti-Collagen III (Southern Biotech, Birmingham, AL, USA, #1330-01, dilution: 1:20) with donkey anti-goat IgG—HRP (Santa Cruz Biotech, Santa Cruz, CA, USA, #sc-20, dilution: 1:20) as a secondary antibody; rat monoclonal (A3-1) anti-F4/80 (Abcam, Cambridge, MA, USA, #ab6640), diluted 1:100 with biotinylated rabbit anti-rat IgG (Vector Laboratories, Burlingame, CA, USA, #BA-4001, dilution 1:100) as a secondary antibody.

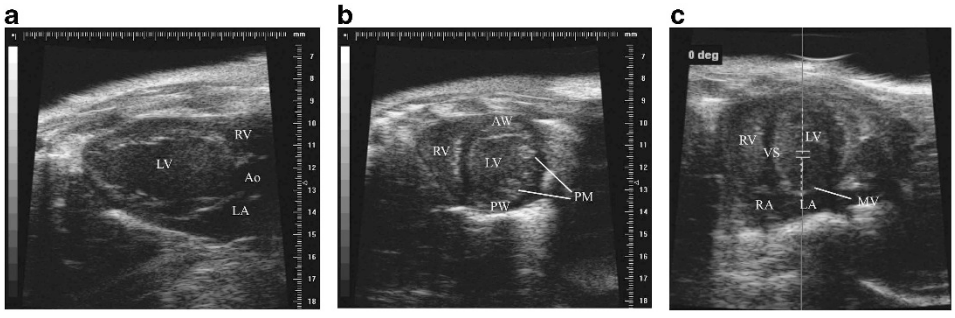

Figure 1 Echocardiographic images. Representative echocardiographic acquisitions of parasternal long-axis (**a**), parasternal short-axis (**b**) and apical four chamber view (**c**) at baseline. In **c**, the sample volume position is shown in order to have the mitral inflow as parallel to the transducer as possible. Ao, aorta; AW, anterior wall; LV, left ventricle; LA, left atrium; MV, mitral valve; PW, posterior wall; PM, papillary muscles; RA, right atrium; RV, right ventricle; VS, ventricular septum. A full color version of this figure is available at the *Hypertension Research* journal online.

Color was developed using NovaRed (Vector Laboratories) followed by hematoxylin counterstain. Coverslips were mounted with Permount mounting media.

Quantitative analysis of extracellular matrix deposition was performed using the MetaVue Image Analysis System (Universal Imaging, Downington, PA, USA), as previously described.[28]

Statistical analysis

Statistical comparisons between baseline and 2 or 4 weeks post surgery were performed using non-parametric Wilcoxon matched pairs test, when possible, or Mann–Whitney test. Results are expressed as medians with interquartile range of multiple experiments. Statistical significance was established at two-tailed $P<0.05$. Linear regression analysis was used to analyze the relationship between histological changes and echocardiographic parameters.

RESULTS

Figure 2 shows a representative image of the plastic cuff placement around the renal artery (Figure 2a); also shown is the echocardiographic demonstration of the cuff location (Figure 2b). As per the protocol design, all mice showed a significant elevation of systolic BP (baseline: 99.26 ± 1.09 mm Hg; 2 weeks: 140.90 ± 7.64 mm Hg, 4 weeks: 147.52 ± 5.91 mm Hg, $P<0.05$ vs baseline), diastolic BP (baseline: 69.91 ± 1.84 mm Hg; 2 weeks: 97.57 ± 5.15 mm Hg, 4 weeks: 103.77 ± 5.92 mm Hg, $P<0.05$ vs baseline) as well as mean arterial BP (baseline: 79.39 ± 0.89 mm Hg; 2 weeks: 111.71 ± 5.95 mm Hg, 4 weeks: 118.03 ± 5.80 mm Hg, $P<0.05$ vs baseline).

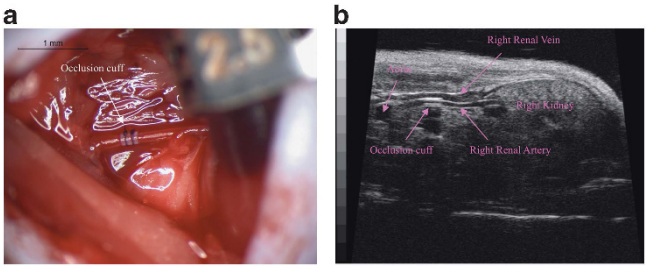

Figure 2 Renovascular hypertension mouse model. Representative surgical image of the occlusion cuff placement around the right renal artery (**a**), and ultrasound image of the cuff around the renal artery 2 weeks after surgery (**b**).

Echocardiography

Two weeks after the induction of renal artery stenosis, there was an increase in LV muscle mass (Figure 3a), that was more pronounced 4 weeks after the induction of renal artery stenosis, and significantly different when compared with baseline. Accordingly, as early as 2 weeks after the induction of renal artery stenosis, there was a decrease in left ventricular end-diastolic volume (LVEDV) and an increase in LVEF, with a CO that was not different from baseline (Figure 3b).

After the development of hypertension, animals showed an abnormal diastolic function as measured using standard clinical parameters. Specifically, at 4 weeks RVH animals showed shortening of the *E* velocity deceleration time as well as an increase in the E/e', associated with an increase in the *E*/*A* ratio (Figure 4).

Ex-vivo characterization of the effect of RVH in the myocardium

In line with echocardiography findings of increased LV muscle mass, there was an increase in LV wall thickness in RVH compared with controls. Furthermore, and accounting for the difference in wall thickness, the mean myocyte size in RVH animals was significantly larger than a cohort of historic controls (Figure 5a). Trichrome stains demonstrated a significant increase in extracellular matrix deposition (RVH: 8.32 ± 2.96% of tissue area vs controls: 0.16 ± 0.03% of tissue area, $P<0.01$) in response to increased blood pressure in RVH

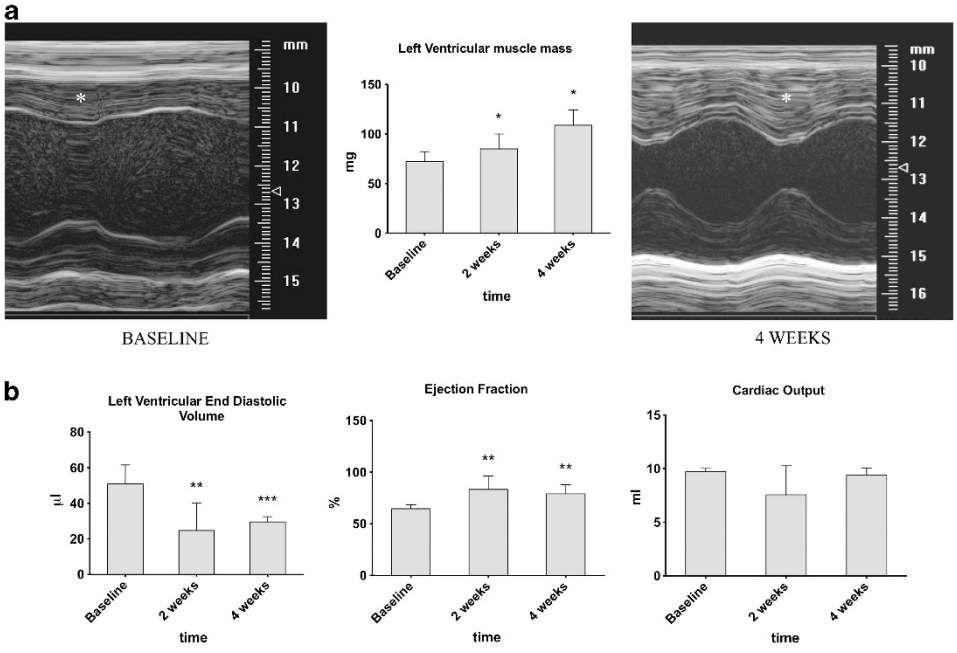

Figure 3 Left ventricular muscle mass and systolic function assessment. (**a**) Representative M-mode echocardiographic acquisitions at baseline and 4 weeks after renal vascular hypertension (RVH) induction. Asterisks indicate the anterior wall of the left ventricle (LV), showing the increased LV muscle thickness in RVH animals; LV muscle mass is quantified in the middle panel. (**b**) Analysis of systolic function parameters, including LV end-diastolic volume, LV ejection fraction and cardiac output at baseline, 2 and 4 weeks post surgery. Data represent medians with interquartile range. *$P<0.05$, **$P<0.01$ and ***$P<0.001$ vs baseline.

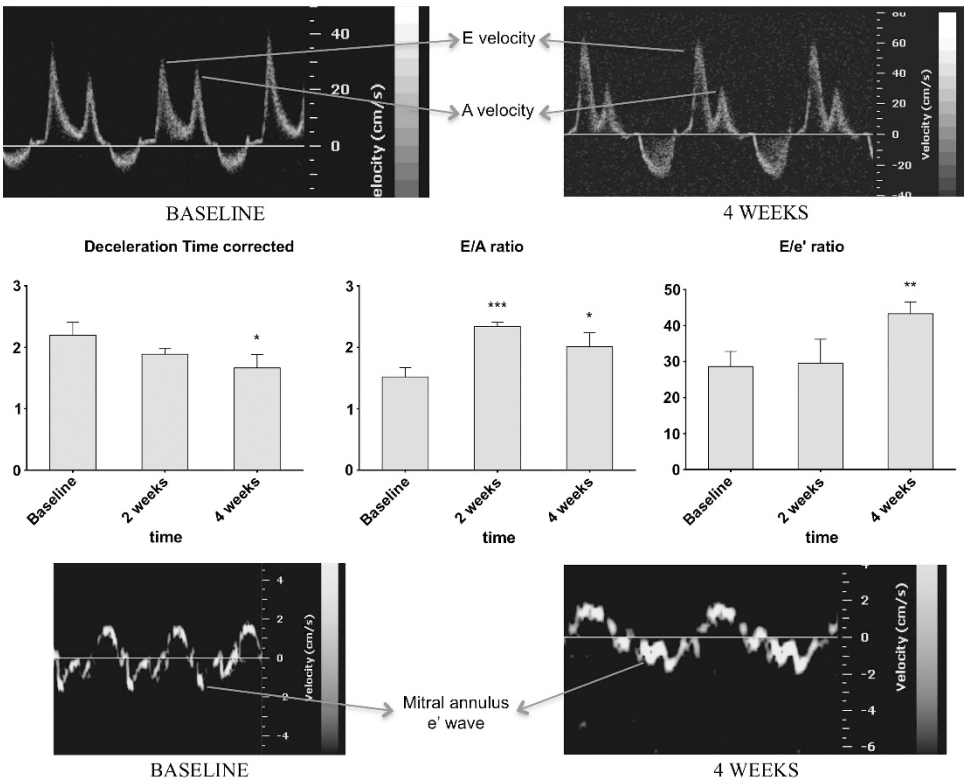

Figure 4 Left ventricular diastolic function assessment. The top panels show representative images of the apical four-chamber mitral valve inflow at baseline and 4 weeks after renal vascular hypertension (RVH) induction, showing *E* wave shortening and a decrease in the mitral inflow deceleration time. Bottom panels show representative images of the mitral annulus tissue Doppler motion at baseline and 4 weeks after RVH induction with a marked decrease of the mitral annulus *e'* wave. Middle panel show the quantification of these signals, using clinically used parameters. *E*: mitral valve *E* velocity, *A*: mitral valve *A* velocity. $^{*}P<0.05$, $^{**}P<0.01$ and $^{***}P<0.001$ vs baseline. A full color version of this figure is available at the *Hypertension Research* journal online.

animals (Figure 5b), which was associated with collagen III staining (Figure 5c) and influx of F4/80-positive macrophages (Figure 5d).

Linear regression analysis did not show a significant correlation between the percentages of tissue area occupied by collagen and any of the evaluated echocardiographic parameters at 4 weeks (% fibrosis vs *E*/*A*: $r^2=0.07$, $P=0.67$; % fibrosis vs *E*/*E'*: $r^2=0.73$, $P=0.064$; % fibrosis vs deceleration time: $r^2=0.27$, $P=0.37$).

DISCUSSION

In this study, we established for the first time the feasibility of a non-invasive assessment of the cardiac manifestations of RVH in a small animal model and their extension to histologic changes in the myocardium. The use of non-invasive imaging for the assessment of cardiac dysfunction will be critical to monitor early disease progression as well as evaluate different therapies.

RVH is the most common of the secondary causes of systemic hypertension,[1] is amenable to specific treatment[2] when identified,and shares many aspects with the idiopathic version of systemic hypertension, such as injury to target organs like the heart.[29–31] Furthermore, much of the morbidity and mortality of hypertension is related to its impact on target organs like the heart.[1] Thus, animal models of RVH serve as an important platform to study not only the mechanisms behind idiopathic hypertensive disease but also the effect of different antihypertensive therapeutic strategies. Our group has previously described a novel small animal model of RVH, based on the use of a plastic cuff to induce unilateral renal artery stenosis.[12,19] In this study, we extend these findings to examine the impact of hypertension non-invasively on cardiac structure and function in a small animal model of renal artery stenosis. The levels of hypertension achieved under our experimental conditions were consistent with the ones recently described by our group.[12] More significant elevation of blood pressure (40–50%) in this experimental model has also been reported by other authors,[32,33] whereas in other studies more moderate increases in blood pressure (10–20%) have been observed.[10,18]

Hypertensive heart disease has been previously shown to affect the myocardium. Indeed, as previously shown,[16] we observed that RVH leads to an increase in LV muscle mass, evident by echocardiography, which is related to an increase in myocyte size. Previous studies showed that induction of hypertension leads to remodeling of the myocardial interstitium that is characterized by increased definition of extracellular matrix.[31,34] In this study, the remodeling of the myocardium was composed of regions of fibrosis as well as an increased influx of F4/80-positive macrophages, which led to remodeling of the myocardium. The lack of correlation between percent fibrosis and echocardiographic parameters, suggests that other factors than just fibrosis may have a role in LV remodeling and diastolic dysfunction.

When using animal models to study development and progression of a clinical disease (hypertension), it is important to use clinically applicable tools. In our study, we chose to use echocardiography, which is the mainstay for clinical assessment of cardiac function[25,26] and on which many clinical decisions regarding therapeutic interventions are based. Traditional ultrasonography with 10–15 MHz transducers has been used to assess cardiac function in murine models of cardiovascular disease.[27,35,36] However, the limit of

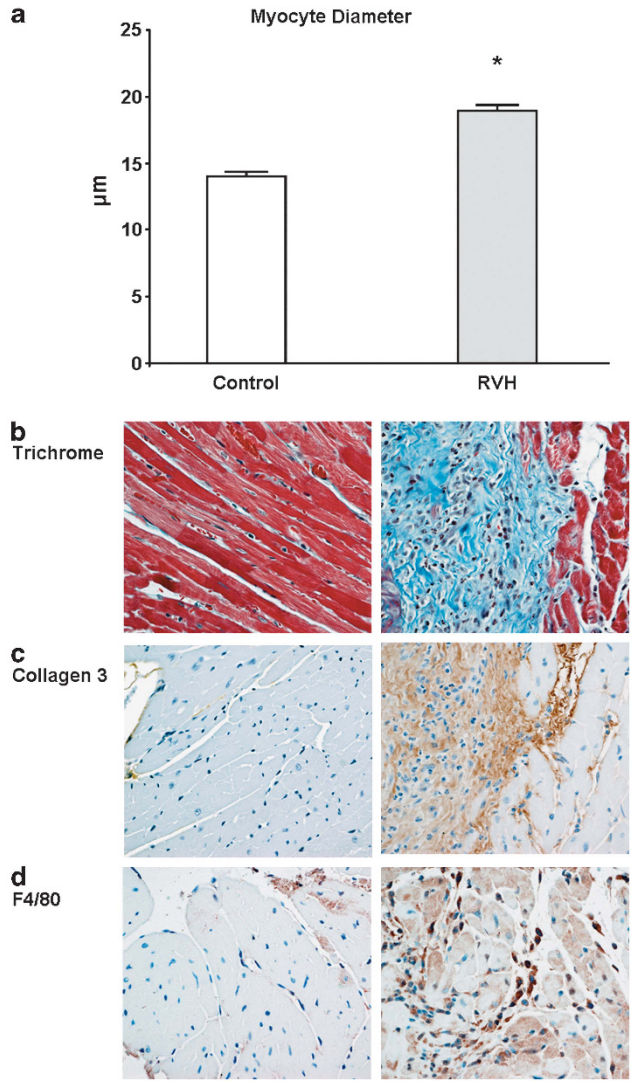

Figure 5 Left ventricular histological assessment. (**a**) Analysis of myocyte diameter in control and renal vascular hypertension (RVH) animals 4 weeks after surgery. Data represent mean ± s.e.m. $^*P<0.05$ vs control. (**b–d**) Representative images of histological staining of myocardium from control animals (left panel) and RVH animals (right panel): (**b**) Masson's Trichrome, (**c**) collagen 3, (**d**) F4/80 + macrophages.

spatial resolution has prevented characterization of structures <0.3 mm.[37] Moreover, low temporal resolution (<200 frame per second) made it difficult to study the movements of the myocardium and valves, as well as quantify cavity dimensions in animals with high heart rates.

Recently, novel developments in ultrasonography with improvements in high spatial (30 µm) and temporal (up to 1000 frame per s in M-Mode imaging) resolution made possible a more accurate assessment of LV systolic, diastolic and vascular function in murine models of cardiovascular disease.[38,39] Actually, the rapid attenuation of high-frequency (30 MHz) sound waves and the consequent shallow tissue penetration (7–10 mm) are ideal for ultrasonography in small size animals with thin tissue.

Previous studies in small animal models have emphasized echocardiography to assess LV systolic function, which is the main determinant of patient survival, and have provided important insights on the development and progression of the hypertensive disease. In fact, we observed an early increase in left ventricular end-systolic volume (LVESV) that might suggest a compensatory mechanism to offset a decrease in LVEDV, in order to increase LVEF and preserve CO. Recently, several studies have reported echocardiographic parameters of systolic function in 2K1C mice models.[10,40] In our experimental conditions, we observed an increase in LVEF that has not been reported previously, with a CO consistent with the data already published.[11,16,40] However, there are differences, such as the time point of the echocardiographic evaluation, the level of hypertension achieved and the mouse strains used that could explain the discrepancy between studies. Here we describe, for the first time, the diastolic function profile of systemic hypertension in small animals after induction of renal artery stenosis. In addition to observations of diastolic pathophysiology in RVH, this study provides a non-invasive platform that can be used to monitor the effect of different therapeutic strategies as they are being developed.

The increase in afterload seen in hypertension leads to an increase in LV end-diastolic pressure, and by LaPlace's law, to an increase in muscle thickness and remodeling of the myocardium, both at the level of the myocyte and the interstitium, which are considered the main determinants of diastolic relaxation abnormalities. Clinically, diastolic dysfunction has been classified into four different grades:[26] (1) abnormal relaxation; (2) pseudo-normalization; (3) reversible restrictive and (4) irreversible restrictive. In our study, the diastolic dysfunction observed appeared to mostly correspond to stages 3 or 4 (restrictive filling). As diastolic dysfunction progresses rapidly in mice,[41] multiple different Doppler patterns may exist in the same group of surgically modeled mice and this may lead to a different progression pattern of the stages of diastolic dysfunction in mice. Thus, the assessment of diastolic function was not based on a single variable but rather on a combination of parameters (deceleration time, E/e' ratio, E/A ratio), which increased the validity of the findings. The early changes in LVEF likely represent a compensatory mechanism for the diastolic dysfunction, suggesting that in the stages studied, our model reflects a pure diastolic dysfunction model.

Anesthesia depresses contraction, heart rate and autonomic reflex control. It would be, then, preferable to perform echocardiographic studies in conscious rather than sedated animals. However, it should be noted that at physiologic (conscious) heart rates, the *E* and *A* waves of the transmitral valve inflow are typically fused, which makes the analysis of diastolic function difficult. Common regimens of anesthesia for echocardiograhic evaluation include ketamine-xylazine,[10,16] ketamine-acepromazine,[42] pentobarbital[16] and inhalation agents, such as isoflurane. These agents differ with respect to duration and depth of sedation, with altered consequences on cardiac physiology, systolic and diastolic function. In this study, we chose to use isoflurane as it causes less depression of cardiac function and heart rate, providing more reproducible results.[16]

Notably, due to considerable variability in heart rates among mouse strains as well as phenotypic variation within a strain, including variation in anesthetic response,[35] there may be differences in the absolute values of systolic and diastolic parameters measured between small animal strains,[43,44] again underscoring that diastolic function should be assessed using a number of parameters, as done in the clinic setting. These features highlight the importance of longitudinal assessment of diastolic function, preferably under the same anesthesia regimens, as done in this study.

Limitations of the study

In our model, we observed a significant increase in LV muscle mass as early as 2 weeks after the induction of renal artery stenosis. This

time-frame, from the development of hypertension to increases in LV mass, is faster than what we would see in the clinical population. Furthermore, we did not observe the abnormal relaxation or pseudo-normalization stages of diastolic dysfunction in our study, but we cannot exclude that milder grades of diastolic dysfunction are present earlier than 2 weeks after induction of renal artery stenosis, which could have been detected if animals had been studied at earlier time points.

In summary, in this study, we described the diastolic function profile in a small animal model of RVH, using non-invasive high-resolution ultrasonography. Use of such non-invasive modalities will have a critical role in both monitoring disease progression as well as assessing the effect of therapeutic interventions.

ACKNOWLEDGEMENTS

This study was supported in part by the National Institutes of Health grants PPG-HL085307 and HL88048, Novartis and the Mayo Foundation.

1 Roger VL, Go AS, Lloyd-Jones DM, Benjamin EJ, Berry JD, Borden WB, Bravata DM, Dai S, Ford ES, Fox CS, Fullerton HJ, Gillespie C, Hailpern SM, Heit JA, Howard VJ, Kissela BM, Kittner SJ, Lackland DT, Lichtman JH, Lisabeth LD, Makuc DM, Marcus GM, Marelli A, Matchar DB, Moy CS, Mozaffarian D, Mussolino ME, Nichol G, Paynter NP, Soliman EZ, Sorlie PD, Sotoodehnia N, Turan TN, Virani SS, Wong ND, Woo D, Turner MBAmerican Heart Association Statistics C, Stroke Statistics S. Heart disease and stroke statistics—2012 update: a report from the American Heart Association. *Circulation* 2012; **125**: e2–e220.
2 Textor SC. Current approaches to renovascular hypertension. *Med Clin N Am* 2009; **93**: 717–732. Table of Contents.
3 Brilla CG. Regression of myocardial fibrosis in hypertensive heart disease: diverse effects of various antihypertensive drugs. *Cardiovasc Res* 2000; **46**: 324–331.
4 Brilla CG, Funck RC, Rupp H. Lisinopril-mediated regression of myocardial fibrosis in patients with hypertensive heart disease. *Circulation* 2000; **102**: 1388–1393.
5 Brilla CG, Janicki JS, Weber KT. Cardioreparative effects of lisinopril in rats with genetic hypertension and left ventricular hypertrophy. *Circulation* 1991; **83**: 1771–1779.
6 Cingolani HE, Rebolledo OR, Portiansky EL, Perez NG, Camilion de Hurtado MC. Regression of hypertensive myocardial fibrosis by Na(+)/H(+) exchange inhibition. *Hypertension* 2003; **41**: 373–377.
7 van Zwieten PA. The influence of antihypertensive drug treatment on the prevention and regression of left ventricular hypertrophy. *Cardiovasc Res* 2000; **45**: 82–91.
8 Goldblatt H, Lynch J, Hanzal RF, Summerville WW. Studies on experimental hypertension: I. The production of persistent elevation of systolic blood pressure by means of renal ischemia. *J Exp Med* 1934; **59**: 347–379.
9 Eng E, Veniant M, Floege J, Fingerle J, Alpers CE, Menard J, Clozel JP, Johnson RJ. Renal proliferative and phenotypic changes in rats with two-kidney, one-clip Goldblatt hypertension. *Am J Hypertens* 1994; **7**: 177–185.
10 Griol-Charhbili V, Sabbah L, Colucci J, Vincent MP, Baudrie V, Laude D, Elghozi JL, Bruneval P, Picard N, Meneton P, Alhenc-Gelas F, Richer C. Tissue kallikrein deficiency and renovascular hypertension in the mouse. *Am J Physiol Regul Integr Comp Physiol* 2009; **296**: R1385–R1391.
11 Signolet I, Gasser B, Bousquet P, Monassier L. Echocardiography in conscious 1K,1C Goldblatt rabbits reveals typical features of human hypertensive ventricular diastolic dysfunction. *Int J Cardiol* 2009; **132**: 135–137.
12 Cheng J, Zhou W, Warner GM, Knudsen BE, Garovic VD, Gray CE, Lerman LO, Platt JL, Romero JC, Textor SC, Nath KA, Grande JP. Temporal analysis of signaling pathways activated in a murine model of two-kidney, one-clip hypertension. *Am J Physiol* 2009; **297**: F1055–F1068.
13 Atlas SA. The renin-angiotensin aldosterone system: pathophysiological role and pharmacologic inhibition. *J Manag Care Pharm* 2007; **13** (8 Suppl B), 9–20.
14 Borges GR, Salgado HC, Silva CA, Rossi MA, Prado CM, Fazan R Jr.. Changes in hemodynamic and neurohumoral control cause cardiac damage in one-kidney, one-clip hypertensive mice. *Am J Physiol Regul Integr Comp Physiol* 2008; **295**: R1904–R1913.
15 Collins KA, Korcarz CE, Lang RM. Use of echocardiography for the phenotypic assessment of genetically altered mice. *Physiol Genomics* 2003; **13**: 227–239.
16 Yang XP, Liu YH, Rhaleb NE, Kurihara N, Kim HE, Carretero OA. Echocardiographic assessment of cardiac function in conscious and anesthetized mice. *Am J Physiol* 1999; **277** (5 Pt 2), H1967–H1974.
17 Lorenz JN, Lasko VM, Nieman ML, Damhoff T, Prasad V, Beierwaltes WH, Lingrel JB. Renovascular hypertension using a modified two-kidney, one-clip approach in mice is not dependent on the alpha1 or alpha2 Na-K-ATPase ouabain-binding site. *Am J Physiol* 2011; **301**: F615–F621.
18 Wiesel P, Mazzolai L, Nussberger J, Pedrazzini T. Two-kidney, one clip and one-kidney, one clip hypertension in mice. *Hypertension* 1997; **29**: 1025–1030.
19 Warner GM, Cheng J, Knudsen BE, Gray CE, Deibel A, Juskewitch JE, Lerman LO, Textor SC, Nath KA, Grande JP. Genetic deficiency of Smad3 protects the kidneys from atrophy and interstitial fibrosis in 2K1C hypertension. *Am J Physiol* 2012; **302**: F1455–F1464. .
20 Rodriguez-Porcel M, Gheysens O, Chen IY, Wu JC, Gambhir SS. Image-guided cardiac cell delivery using high-resolution small-animal ultrasound. *Mol Ther* 2005; **12**: 1142–1147.
21 Collins KA, Korcarz CE, Shroff SG, Bednarz JE, Fentzke RC, Lin H, Leiden JM, Lang RM. Accuracy of echocardiographic estimates of left ventricular mass in mice. *Am J Physiol Heart Circ Physiol* 2001; **280**: H1954–H1962.
22 Kiatchoosakun S, Restivo J, Kirkpatrick D, Hoit BD. Assessment of left ventricular mass in mice: comparison between two-dimensional and m-mode echocardiography. *Echocardiography* 2002; **19**: 199–205.
23 Gardin JM, Siri FM, Kitsis RN, Edwards JG, Leinwand LA. Echocardiographic assessment of left ventricular mass and systolic function in mice. *Circ Res* 1995; **76**: 907–914.
24 Trambaiolo P, Tonti G, Salustri A, Fedele F, Sutherland G. New insights into regional systolic and diastolic left ventricular function with tissue Doppler echocardiography: from qualitative analysis to a quantitative approach. *J Am Soc Echocardiogr* 2001; **14**: 85–96.
25 Nishimura RA, Abel MD, Hatle LK, Tajik AJ. Assessment of diastolic function of the heart: background and current applications of Doppler echocardiography. Part II. Clinical studies. *Mayo Clin Proc* 1989; **64**: 181–204.
26 Oh JK, Appleton CP, Hatle LK, Nishimura RA, Seward JB, Tajik AJ. The noninvasive assessment of left ventricular diastolic function with two-dimensional and Doppler echocardiography. *J Am Soc Echocardiogr* 1997; **10**: 246–270.
27 Schmidt AG, Gerst M, Zhai J, Carr AN, Pater L, Kranias EG, Hoit BD. Evaluation of left ventricular diastolic function from spectral and color M-mode Doppler in genetically altered mice. *J Am Soc Echocardiogr* 2002; **15** (10 Pt 1), 1065–1073.
28 Diaz Encarnacion MM, Griffin MD, Slezak JM, Bergstralh EJ, Stegall MD, Velosa JA, Grande JP. Correlation of quantitative digital image analysis with the glomerular filtration rate in chronic allograft nephropathy. *Am J Transplant* 2004; **4**: 248–256.
29 Hocher B, Godes M, Olivier J, Weil J, Eschenhagen T, Slowinski T, Neumayer HH, Bauer C, Paul M, Pinto YM. Inhibition of left ventricular fibrosis by tranilast in rats with renovascular hypertension. *J Hypertens* 2002; **20**: 745–751.
30 Challah M, Nicoletti A, Arnal JF, Philippe M, Laboulandine I, Allegrini J, Alhenc-Gelas F, Danilov S, Michel JB. Cardiac angiotensin converting enzyme overproduction indicates interstitial activation in renovascular hypertension. *Cardiovasc Res* 1995; **30**: 231–239.
31 Baxter GF. Inhibition by diltiazem of left ventricle collagen proliferation during renovascular hypertension development in rats. *J Pharm Pharmacol* 1992; **44**: 277–278.
32 Lazartigues E, Lawrence AJ, Lamb FS, Davisson RL. Renovascular hypertension in mice with brain-selective overexpression of AT1a receptors is buffered by increased nitric oxide production in the periphery. *Circ Res* 2004; **95**: 523–531.
33 Cervenka L, Vaneckova I, Maly J, Horacek V, El-Dahr SS. Genetic inactivation of the B2 receptor in mice worsens two-kidney, one-clip hypertension: role of NO and the AT2 receptor. *J Hypertens* 2003; **21**: 1531–1538.
34 Dussaillant GR, Gonzalez H, Cespedes C, Jalil JE. Regression of left ventricular hypertrophy in experimental renovascular hypertension: diastolic dysfunction depends more on myocardial collagen than it does on myocardial mass. *J Hypertens* 1996; **14**: 1117–1123.
35 Roth DM, Swaney JS, Dalton ND, Gilpin EA, Ross J Jr. Impact of anesthesia on cardiac function during echocardiography in mice. *Am J Physiol Heart Circ Physiol* 2002; **282**: H2134–H2140.
36 Schaefer A, Klein G, Brand B, Lippolt P, Drexler H, Meyer GP. Evaluation of left ventricular diastolic function by pulsed Doppler tissue imaging in mice. *J Am Soc Echocardiogr* 2003; **16**: 1144–1149.
37 Mahmoud AM, Sandoval C, Teng B, Schnermann JB, Martin KH, Jamal Mustafa S, Mukdadi OM. High-resolution vascular tissue characterization in mice using 55 MHz ultrasound hybrid imaging. *Ultrasonics* 2012; **53**: 727–738.
38 Christopher DA, Burns PN, Starkoski BG, Foster FS. A high-frequency pulsed-wave Doppler ultrasound system for the detection and imaging of blood flow in the microcirculation. *Ultrasound Med Biol* 1997; **23**: 997–1015.
39 Goertz DE, Yu JL, Kerbel RS, Burns PN, Foster FS. High-frequency 3-D color-flow imaging of the microcirculation. *Ultrasound Med Biol* 2003; **29**: 39–51.
40 Gao J, Bellien J, Gomez E, Henry JP, Dautreaux B, Bounoure F, Skiba M, Thuillez C, Richard V. Soluble epoxide hydrolase inhibition prevents coronary endothelial dysfunction in mice with renovascular hypertension. *J Hypertens* 2011; **29**: 1128–1135.
41 Gao S, Ho D, Vatner DE, Vatner SF. Echocardiography in mice. *Curr Protoc Mouse Biol* 2011; **1**: 71–83.
42 Rottman JN, Ni G, Khoo M, Wang Z, Zhang W, Anderson ME, Madu EC. Temporal changes in ventricular function assessed echocardiographically in conscious and anesthetized mice. *J Am Soc Echocardiogr* 2003; **16**: 1150–1157.
43 Ram R, Mickelsen DM, Theodoropoulos C, Blaxall BC. New approaches in small animal echocardiography: imaging the sounds of silence. *Am J Physiol Heart Circ Physiol* 2011; **301**: H1765–H1780.
44 Hoit BD, Kiatchoosakun S, Restivo J, Kirkpatrick D, Olszens K, Shao H, Pao YH, Nadeau JH. Naturally occurring variation in cardiovascular traits among inbred mouse strains. *Genomics* 2002; **79**: 679–685.